Optics and Lasers in Engineering 54 (2014) 1–7

Contents lists available at ScienceDirect

Optics and Lasers in Engineering

journal homepage: www.elsevier.com/locate/optlaseng

Visual-based spatter detection during high-power disk laser welding ☆

Deyong You [a,b], Xiangdong Gao [a,*], Seiji Katayama [b]

[a] Faculty of Electromechanical Engineering, Guangdong University of Technology, No. 100 West Waihuan Road, Higher Education Mega Center, Panyu District, Guangzhou 510006, China
[b] Joining and Welding Research Institute, Osaka University, 11-1 Mihogaoka, Ibaraki, Osaka 567-0047, Japan

ARTICLE INFO

Article history:
Received 13 December 2011
Received in revised form
4 September 2013
Accepted 15 September 2013
Available online 24 October 2013

Keywords:
High power laser welding
Spattering
Visual detection
Quality inspection

ABSTRACT

The spatters created during laser welding are considered as essential information for welding quality inspection. This paper proposes a laser welding quality inspection method based on the high-speed visual detection. A high-power (10 kW) disk laser bead-on-plate welding of Type 304 austenitic stainless workpiece was carried out and two high-speed cameras were used to capture the spatter images. The first one was used to measure the near infrared (IR) light emitted from a molten pool, and the second was utilized to measure the ultraviolet (UV) light and visible light. By comparing the images captured from two different cameras, it was found that the measurement of UV light and visible light was more appropriate for spatter detection. Based on image process technology, a novel spatter detection algorithm was presented. A shape similarity function and angle similarity function of the spatters were established for spatter recognition by defining the spatter features, such as centroid position, gray-value, average gray-value and radius. The spatter volume, spatter gray-value and spatter radius were used to evaluate the welding quality. By comparing the spatter information with the molten pool width, this paper investigates the internal relationship between the welding quality and the spatter feature parameters. Experimental results proved that the proposed spatter feature extraction method could guarantee an accurate evaluation on the quality of high-power disk laser welding. In addition it was demonstrated in this study that, by using high-speed visual detection and image processing technology, the quantities and feature of spatters could be measured during the welding process.

1. Introduction

Laser welding has been widely used for its advantages due to high intensity heat sources in narrowly focusing a laser beam to a small area, which is instrumental in realizing deep-penetration and high-speed welding, and improving mechanical properties [1–5]. An effective method for monitoring the welding process is essential to improve welding quality [6–8]. In order to optimize the productivity of laser welding, electromagnetic emissions from the weld zone, such as reflected light, thermal radiation and plasma radiation, are the most important information during on-line monitoring [9,10]. Several fundamental studies on plasma monitoring have been performed to evaluate the stability of laser welding [11,12]. High-speed photography has been proved to be an effective method in analyzing the structure and dynamic behavior of a keyhole during the laser welding process [13,14]. Also, metal spatters incurred during laser welding affect the molten pool shape and the welding quality. During laser welding, spattering refers to the scattering of fluid metal made by laser-induced plume steams from the keyhole. Effective monitoring and control over metal spatters are prerequisites to the production of high-quality welds. Sehun Rhee in Korea used IR and UV sensors to collect plasma and spatter signals during welding, and analyzed them by way of multiple characteristics pattern recognition in order to evaluate welding quality [15,16]. A study shows the optimal model for estimating the amount of spatter when considering arc extinction in short circuit transfer mode, and the optimal model for estimating spatter rate using an artificial neural network in the short circuit transfer region of GMAW [17,18]. Also some methods for measuring spatter in gas metal arc welding by optical monitoring of the weld pool and surrounding area via a high-frame-rate camera were proposed and have been proven to be effective [19]. Pattern recognition and Kalman filter algorithm were adopted to enhance spatter recognition accuracy and the effectiveness of spatter feature analysis [20]. Some research works have been conducted to monitor the laser welding defects like spatters [21,22]. It was possible to accurately position the welding spatter by using image recognition technology, thus eliminating the spatter influence on molten pool recognition [23].

Previous research works have proved that keyhole wall shows smooth distribution even at a stable status, and only a few small

☆This work is an expanded version of the paper published at International Conference on Advanced Design and Manufacturing Engineering (ADME) 2011 in Guangzhou, China, September 16–18, 2011.

* Corresponding author. Tel.: +86 137 11457326; fax: +86 208 5215998.
E-mail address: gaoxd666@126.com (X. Gao).

0143-8166/$ - see front matter © 2013 Elsevier Ltd. All rights reserved.
http://dx.doi.org/10.1016/j.optlaseng.2013.09.010

spatters are produced inside the keyhole [24]. However, keyhole wall shows distinguishable wave distribution at an unstable status [25]. If the unstable status remains, molten metal will be separated from the molten pool because of vaporized pressure and produce spatters of large size [26]. Since spatters are from the inside of the molten pool, the amount of molten metal within weld seam area will surely reduce when spatters of large size are produced. This results in external defects (such as underfill or lack of fusion) of weld seam [27]. In addition, the production of large-sized spatters indicates an unstable status inside the keyhole. Especially, there is wave distribution of the keyhole wall, which might also result in internal defects (such as porosity) of weld seam [27]. Therefore, the key for spatter detecting is to accurately identify spatters of large size. Up to the present time, however, accurate quantification of spatter during laser welding process is still a formidable task. In this work the high-power disk laser bead-on-plate welding of Type 304 austenitic stainless steel plates was carried out and two high-speed cameras were used to capture the spatter images of welding process in order to extract instantaneous variation of metal spatters. It was followed by the performance of image pre-processing algorithm to extract spatter information of each image, including spatter centroid, area, grayscale, average grayscale and direction. A spatter searching matrix was then built up accordingly. The spatters generated at time t and prior to time t could be distinguished by comparing the spatters feature similarity functions. The radiuses of spatters were extracted to calculate the volume of spatters generated at time t, which was used as quantification information for evaluating the welding quality. It was also demonstrated that the spatters gray-value could be used for welding quality inspection.

2. Experimental setup

The experimental setup includes a Motorman 6-axis robot, high-power disk laser TruDisk-10003(10 kW), NAC high-speed camera (2000 f/s), shielding gas (argon), and Type 304 austenitic stainless workpiece ($150\times100\times10\ \mathrm{mm}^3$). The structure of the experimental setup is shown in Fig. 1. The beam diameter of laser focus was 480 μm, and the laser wavelength was 1030 nm. The gas flow was 40 L/min while the nozzle angle was 45°. Welding speed was 4.5 m/min. The workpiece was driven by a precise servo motor installed on the working table. The spectral band-pass filter setup on camera 1 was 320–750 nm (measurement of UV and visible light induced plume and spatter), while the other setup on camera 2 was 960–990 nm (measurement of near IR light emitted from the molten pool). The response curves of different filters are shown in Fig. 2. As shown in Fig. 2(b), there are two optical filters set up on camera 2 in order to capture the near IR light. The angle

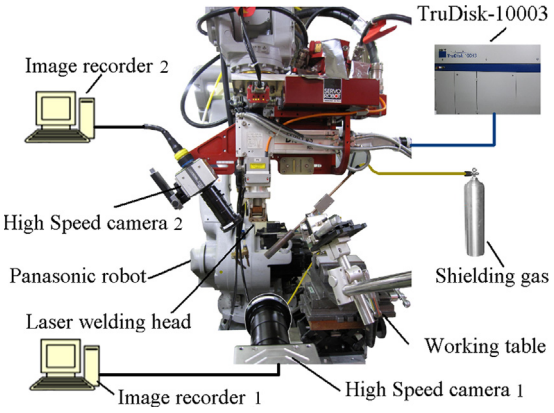

Fig. 1. Experimental setup of high-power disk laser bead-on-plate welding.

of camera 1 was 0°, while that of camera 2 was 75°. The spatter images, shown in Figs. 3 and 4, were captured by different cameras. The image resolution was 512 pixel × 512 pixel. The images shown in Fig. 3 contained clear information of plume (UV light) and spatters (visible light). The images shown in Fig. 4 reflected detail information of molten pool (IR band). The images captured by camera 1 are used for spatter detection, while images captured by camera 2 are more conducive to analyze thermal distribution of molten pool. The image sequence captured by high-speed camera 1 is shown in Fig. 5. By using high-speed photography and image processing technology the spatters could be detected during the laser welding process. Thus the detailed information of spatters, such as spatter volume, spatter gray-value and spatter radius, could be extracted to evaluate the laser welding quality.

3. Extraction and quantification of spatter features

For the convenience of image processing, the spatter images were converted to grayscale images, which are shown in Fig. 6(a) and (d). Also, the grayscale images were pre-processed to eliminate plume information in order to obtain accurate spatter features, which are shown in Fig. 6(b) and (e). An individual spatter j at sample time t was defined as $c_t(i,j)$. This spatter j contained six characteristics ($i=1,2,\ldots,6$), which were centroid positions ($c_t(1,j)$, $c_t(2,j)$), area $c_t(3,j)$, gray-value $c_t(4,j)$, average gray-value $c_t(5,j)$ and radius $c_t(6,j)$. The characteristics were defined as follows:

$$c_t(1,j)=\frac{\sum_{x,y\in D_j}\mathbf{P}_t(x,y)x}{\sum_{x,y\in D_j}\mathbf{P}_t(x,y)},$$

$$c_t(2,j)=\frac{\sum_{x,y\in D_j}\mathbf{P}_t(x,y)y}{\sum_{x,y\in D_j(t)}\mathbf{P}_t(x,y)},\quad x,y=1,\ldots,512 \tag{1}$$

$$c_t(3,j)=d_j(t),\ \ c_t(4,j)=\sum_{x,y\in D_j(t)}\mathbf{P}_t(x,y),\quad x,y=1,\ldots,512 \tag{2}$$

$$c_t(5,j)=\frac{\sum_{x,y\in D_j(t)}\mathbf{P}_t(x,y)}{d_j(t)},$$

$$c_t(6,j)=\frac{\sum_{x,y\in E_j(t)}\sqrt{(x-c_{1,j})^2+(y-c_{2,j})^2}}{e_j(t)},\quad x,y=1,\ldots,512 \tag{3}$$

where $c_t(i,j)$ is the data matrix of spatters on the images captured at time t, $\mathbf{P}_t$ is the spatter image at time t, and $\mathbf{P}_t(x,y)$ is the gray-value of position (x,y); D_j and E_j represent the covering area and edge of spatter j, respectively, while $d_t(j)$ and $e_t(j)$ are the pixel numbers of the covering area and edge of spatter j at time t respectively.

To recognize the spatter generated at time t, spatter searching matrix $o_t(u,\ v)$ was established, which contained information of all spatters generated before time t (including time t), such as centroid positions ($o_t(1,\ v)$, $o_t(2,\ v)$), area $o_t(3,\ v)$, gray-value $o_t(4,\ v)$, average gray-value $o_t(5,\ v)$ and radius $o_t(6,\ v)$.

In order to distinguish the spatters generated at time t from the spatters generated prior to time t, shape similarity function $simi(v,j)$ and angle similarity function $dgsimi(v,j)$ of the spatters were established which are expressed in Eqs. (4) and (5). Both functions were used for comparing the spatter feature similarity between searching matrix $o_{t-1}(u,\ v)$ at time $t-1$ and data matrix $c_t(i,\ j)$ at time t. By using the shape similarity function and angle similarity function, it is possible to extract the position and feature parameters of the new spatter generated at time t, and add its new information to $o_t(u,\ v)$ as searching basis at time $t+1$. The process